*Journal of The Electrochemical Society*, **152** (5) A989-A995 (2005)
0013-4651/2005/152(5)/A989/7/$7.00 © The Electrochemical Society, Inc.



# Electrochemical and Spectroscopic Properties of Electrospun PAN-Based Fibrous Polymer Electrolytes

**S. W. Choi,[a] J. R. Kim,[b] S. M. Jo,[b,z] W. S. Lee,[b] and Y.-R. Kim[a]**

[a]*Department of Chemistry, Yonsei University, Seoul 120-749, Korea*
[b]*Polymer Hybrid Research Center, Korea Institute of Science and Technology, Seoul 136-791, Korea*

Microporous fibrous polymer electrolytes were prepared by immersing electrospun poly(acrylonitrile) (PAN)-based fibrous membranes into lithium salt-based electrolytes. They showed high ionic conductivities of up to $1.0 \times 10^{-3}$ S/cm at 20°C, and sufficient electrochemical stabilities of up to 4.5 V. Their ion conduction depended on the physicochemical properties of the lithium salt-based electrolytes trapped in pores, as well as on the interactions among the $Li^+$ ion, the carbonate, and the PAN. From the Fourier transform-Raman data, lithium ion transport was mainly achieved by the lithium salt-based electrolytes in pores via the interaction between the $Li^+$ ion and the C=O group of carbonate molecules, and was also affected by the PAN through the interaction between the $Li^+$ ion and the C≡N groups of PAN. Their electrochemical stabilities were enhanced by the swelling of the electrospun PAN nanofibers because of the dipolar interaction between the C≡N groups of PAN and the C=O groups of carbonate in the lithium salt-based electrolytes. Prototype cells using electrospun PAN-based fibrous polymer electrolytes thus showed different cyclic performances, according to the composition of the lithium salt-based electrolytes. The prototype cell with 1 M $LiPF_6$-ethylene carbonate/dimethyl carbonate (1/1) showed the highest discharge capacity and the most stable cyclic performance among them.
 [DOI: 10.1149/1.1887166] 

Manuscript submitted February 22, 2004; revised manuscript received November 4, 2004. Available electronically April 7, 2005.

In recent years, phase inversion has been widely studied to make the microporous polymer membrane of polymer electrolytes.[1-3] This process is less sensitive to moisture than solvent casting because a moisture-free environment is required only at the activation step. In addition, polymer electrolytes using a microporous polymer membrane are more mechanically stable than gel polymer electrolytes using the solvent casting method, because the microporous polymer membrane maintains its three-dimensional network structure.

Polyvinylidene fluoride (PVDF) and P(VDF-*co*-HFP) have been mainly utilized as materials for microporous membranes because they are physicochemically and electrochemically stable in a lithium ion polymer battery. The physical and electrochemical properties of the porous PAN membrane using the phase inversion method were recently reported.[4] These show sufficient electrochemical properties, which means that the microporous PAN membrane can also be used as a polymer matrix for polymer electrolytes in a lithium ion polymer battery.

In the gel electrolyte system, a PAN-based polymer electrolyte shows different forms of ion conduction behavior compared with PVDF- or P(VDF-*co*-HFP)-based polymer electrolytes containing cyclic carbonate molecules, such as ethylene carbonate (EC), propylene carbonate (PC), and γ-butyrolactone. It has been confirmed that PAN not only acts as a polymer matrix to maintain the frame of a polymer electrolyte, but also participates in lithium ion transport. From their vibrational spectroscopic data, lithium ions interact with C≡N groups of PAN chains as well as with cyclic carbonate molecules in an electrolyte solution. A vibrational band of $Li^+$-EC complexes generally appeared at 903 $cm^{-1}$, whereas that of free EC molecules appeared at 893 $cm^{-1}$.[5] A new band was also observed at around 2,270 $cm^{-1}$, due to the interaction between the lithium ion and the C≡N groups of PAN.[6] Their intensities and positions varied according to the composition of the PAN-based polymer electrolyte. On the other hand, a PAN-solvent complex was formed from the dipolar interaction between the C≡N groups of PAN and the C=O groups of cyclic carbonate molecules. When the nitrogen atom of the C≡N group of PAN attacked the carbon atom of the C=O group of cyclic carbonate molecules, the electron density around the carbon was enhanced and the C=O bonding became stronger.[7,8] Moreover, the related vibrational band shifted to a higher-frequency region. Electrochemical properties were thus somewhat enhanced by the above mentioned interactions.[9,10] As a result, the PAN-based polymer electrolyte showed a high ionic conductivity and electrochemical stability in the range of the operating voltage. Only a few researchers, however, have studied the PAN-based polymer electrolyte using a microporous membrane.[4] The effect of the porous PAN fibrous membrane on the chemical and electrochemical properties of polymer electrolytes is, in particular, not clearly characterized. Moreover, phase inversion may be an inappropriate technique for preparing the microporous PAN fibrous membrane because PAN is rarely dissolved by a solvent with a low boiling point, which can easily evaporate during drying. Thus, a microporous polymer membrane by phase inversion may be an inhomogeneous membrane with two kinds of structures, like honeycombs or finger-like structures.[11,12]

In a previous study by the authors, the electrospinning technique was proposed for the first time for preparing a microporous polymer matrix for polymer electrolytes.[13] Polymer electrolytes using the electrospun PVDF-based nanofibrous membrane showed sufficient electrochemical properties for application to a lithium ion polymer battery. This paper investigates the microporous electrospun PAN-based fibrous membrane and the electrochemical properties of polymer electrolytes using such a membrane. Interactions between the PAN nanofiber, a lithium ion, and solvent molecules in electrospun PAN-based fibrous polymer electrolytes were characterized using the vibrational spectroscopic technique, to investigate their influence on the electrochemical properties of fibrous polymer electrolytes. The prototype cells of a lithium ion polymer battery using electrospun PAN-based fibrous polymer electrolytes were then fabricated to investigate their cycle performances.

## Experimental

A PAN solution was prepared by dissolving 12 wt % of PAN (Polysciences, Mw = $1.5 \times 10^5$) in *N*, *N*-dimethylacetamide [Merck, high performance liquid chromatography (HPLC) grade]. Microporous electrospun fibrous membranes were prepared using the typical electrospinning method. A silver-coated stainless steel needle was connected to a high-voltage power supply (Bertan, 230). The PAN solution was supplied to a needle using a syringe infusion/withdrawal pump (KD Scientific, model 220), and a high voltage was applied to the end of the needle. The electrospun PAN fibrous matrix was then deposited on a grounded, polished, stainless steel plate. The thickness of the membrane was controlled at 30 μm and vacuum-dried at 60°C overnight.

Electrospun PAN-based fibrous polymer electrolytes were prepared by immersing electrospun PAN fibrous membranes into lithium salt-based electrolytes, such as 1 M $LiPF_6$-EC/ dimethyl carbonate (DMC) (2/1, wt/wt), 1 M $LiPF_6$-EC/DMC (1/1, wt/wt), 1

[z] E-mail: smjo@kist.re.kr

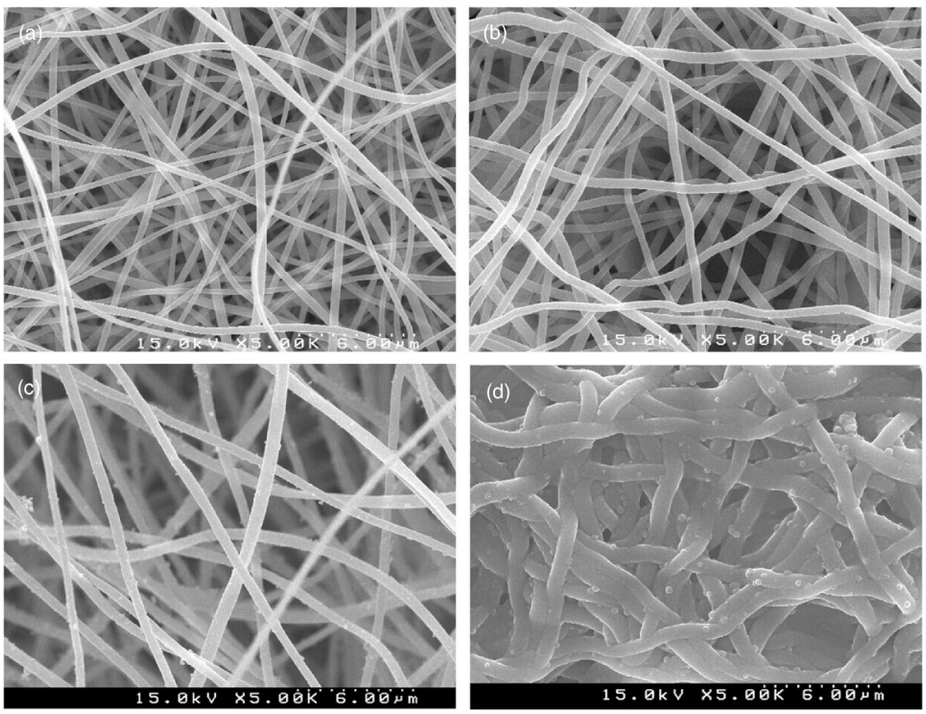


**Figure 1.** SEM images of (a) electrospun PAN fibrous membranes, (b) after storage in an electrolyte solution at 50°C for 12 h, (c) after 100 cycles at the 0.2C/0.2C rate, and (d) after 150 cycles at the 0.2C/0.2C rate.

M $LiPF_6$-EC/ethylmethyl carbonate (EMC) (1/1, wt/wt), 1 M $LiPF_6$-EC/diethyl carbonate (DEC) (1/1, wt/wt), and 1 M $LiPF_6$-EC/DMC/DEC (1/1/1, wt/wt/wt) (Merck, battery grade) at room temperature. This process was carried out in an argon atmosphere ($H_20 < 1$ ppm). A PAN-based gel electrolyte was also prepared for comparison. The PAN-based gel polymer electrolyte consisted of PAN and a lithium-salt-based electrolyte with 1 M $LiPF_6$-EC/DMC (1/1, wt/wt), whose composition is similar to that of the electrospun PAN-based fibrous polymer electrolyte.

The morphology of the electrospun PAN fibrous membrane was observed using a scanning electron microscope (SEM, Hitachi, S-4200). The average fiber diameter of each sample was calculated using software (SigmaScanPro 5.0, SPSS) based on SEM images. The mean pore diameters were measured using a capillary flow porometer (PMI, ver. 7.0). The pressure range was from 0 to 30 psi. The pore size was calculated from the wet and dry flow curves. Perfluoropolyether (called propene, 1,1,2,3,3,3 hexafluoro, oxidized, polymerized) was used as a wetting solvent for this experiment.

Porosity was measured from *n*-buthanol uptake. The electrospun PAN fibrous membrane was immersed in *n*-buthanol for 1 h, after which the mass of the electrospun PAN fibrous membrane before and after its absorption of *n*-buthanol was measured. The porosity of the membrane was calculated using Eq. 1

$$P = \frac{m_a/\rho_a}{m_a/\rho_a + m_p/\rho_p} \quad [1]$$

where $m_p$ is the mass of the dry membrane, $m_a$ is the mass of the buthanol absorbed by the wet membrane, $\rho_p$ is the density of the polymer, and $\rho_a$ is the density of buthanol.

The vibrational spectra of the electrospun PAN-based fibrous polymer electrolytes were obtained using Fourier transform (FT)-Raman spectroscopy (Brucker, RFS-100/s) at a resolution of 1 $cm^{-1}$. The light source was an Nd-YAG laser with a wavelength of 1064 nm. The spectra were collected over the range of 400-3500 $cm^{-1}$ by averaging 300 scans. Individual peaks in FT-Raman were fitted with a trial function consisting of a base line and a Gaussian function (PeakFit 4.0, SPSS).

Ionic conductivity was measured using the impedance technique over the frequency range of 0.1 Hz to 100 kHz, with an ac amplitude of 10 mV and a temperature range of −20 to 60°C using IM6e (Zahner Co., Germany), and interfaced with a personal computer. The conductivity cell was assembled by sandwiching a given electrospun PAN-based fibrous polymer electrolyte between two stainless steel blocking electrodes in a glove box filled with argon gas.

Linear sweep voltammetry was used to determine the electrochemical stability windows of the electrospun PAN-based fibrous polymer electrolytes. The measurement was carried out using a three-electrode electrochemical cell consisting of a nickel working electrode and a lithium reference and counter electrode. An electrochemical analyzer (CHI, model 600) was utilized under the scan rate of 1 mV/s and the potential range of 2-5 V *vs.* $Li^+/Li$.

By sandwiching electrospun PAN-based fibrous polymer electrolytes between a mesocarbon microbead (MCMB) anode (SKC supplied, Korea) and a $LiCoO_2$ cathode (SKC supplied, Korea), a lithium ion cell was assembled in a dry box filled with argon gas ($H_2O < 1$ ppm). The theoretical capacity was estimated from the cycle performance at the 0.2C rate and the composition of the cathode ($LiCoO_2$, conducting material; binder = 90:5:5). The theoretical capacity of the $LiCoO_2$ electrode was about 145 mAh/g. This prototype cell was then vacuum-sealed in an aluminum plastic pouch and stored at 50°C to age, before the cycling test was performed. The charge/discharge tests were conducted with a battery cycler (WBCS3000, WonAtech Co). The cycling performances of the prototype cells were measured at the cutoff voltage of 4.20-2.75 V and at a constant current (1.7 $mA/cm^2$, about the 0.5C rate).

## Results and Discussion

As shown in Fig. 1a, the electrospun PAN-based fibrous membrane consists of nanofibers with smooth surfaces and well-controlled average diameters of 330 nm. It shows a three-dimensional network structure with fully interconnected pores. It has a high porosity of about 90%, however, and a loose pore structure with a large mean pore size of about 2.3 μm, although it was prepared by the deposition of ultrafine fibers. This indicates that dry fibers are deposited by rapid evaporation of the solvent during

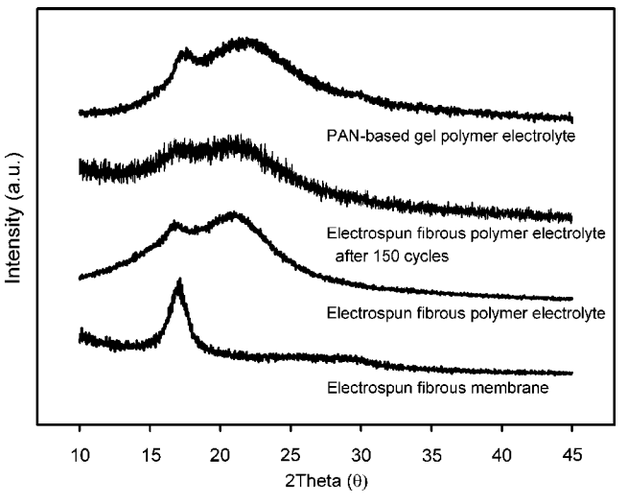


**Figure 2.** XRD patterns of the electrospun PAN-based fibrous membrane, its fibrous polymer electrolytes before and after 150 cycles, and the PAN-based gel polymer electrolyte with 1 M $LiPF_6$-EC/DMC (1/1).

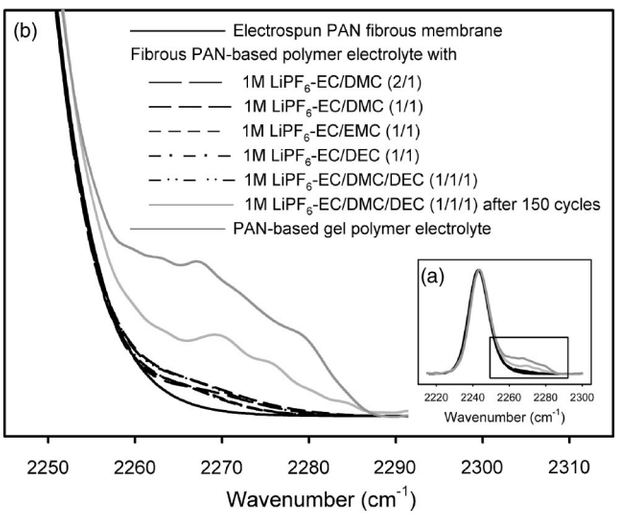


**Figure 3.** The FT-Raman spectra of the C≡N stretching modes of PAN in the electrospun PAN-based fibrous polymer electrolytes before and after 150 cycles, and in the PAN-based gel polymer electrolyte with 1 M $LiPF_6$-EC/DMC (1/1).

electrospinning. Solvent evaporation in electrospinning can be easily controlled. Figure 1b shows the SEM image of the electrospun PAN-based fibrous membrane impregnated with a 1 M $LiPF_6$-EC/DMC (1/1) electrolyte solution at 50°C for 12 h. The electrospun PAN-based fibrous membrane was partially swelled in a lithium salt-based electrolyte, and the average fiber diameter was slightly increased by swelling even after storage for 1 week. The swelling of the PAN-based nanofibers was greatly enhanced, however, during the electrochemical reaction, like the charge/discharge. Figures 1c and d are SEM images of the electrospun PAN-based fibrous membranes in the prototype cells after charge/discharge tests of about 100 and 150 cycles, respectively, were carried out. These prototype cells were assembled with an electrospun PAN-based fibrous polymer electrolyte membrane impregnated with a 1 M $LiPF_6$-EC/DMC (1/1) solution at 50°C for 12 h. The charge/discharge tests were measured at a cutoff voltage of 4.20-2.75 V and at a constant current (1.7 $mA/cm^2$, at about the 0.5C rate). The average fiber diameter of the electrospun PAN-based fibrous membrane after 100 cycles increased more significantly than that impregnated with the electrolyte solution. After 150 cycles, the average fiber diameter of the electrospun PAN-based fibrous membrane remarkably increased by about three times compared with that before the cycling test. It is thus thought that the swelling behavior of the electrospun PAN-based fibrous membrane in the lithium-salt-based electrolyte has some effects on the electrochemical properties and cycling performance of the prototype cell with the electrospun PAN-based fibrous polymer electrolyte.

Figure 2 shows the X-ray diffraction (XRD) patterns of the electrospun PAN-based fibrous membrane, its fibrous polymer electrolytes before and after 150 cycles, and the PAN-based gel electrolyte with 1 M $LiPF_6$-EC/DMC (1/1), for comparison. The electrospun PAN-based fibrous membrane showed a strong peak at around 17° and two weak, broad peaks at around 28 and 55°, which are very similar to that of PAN powder with a hexagonal lattice. A sharp peak at 17° corresponds to the (010) plane with a d-spacing of 5.30 Å.[14,15] PAN powder generally shows a small, sharp peak at around 28°, but the electrospun PAN fibrous membrane showed a weak peak because of its enhanced amorphous phase. The electrospun PAN fibrous membrane, however, retained the crystal structure of the original PAN powder. In the case of the electrospun PAN-based fibrous polymer electrolytes, their strong peaks at around 21° newly appeared, which is assumed to be due to the interaction between the PAN nanofiber and the electrolyte solutions. Although much of the electrolyte solution that penetrated the PAN nanofibers was captured in the amorphous phase of the electrospun PAN fibrous membrane, a slight volume of the electrolyte solution also penetrated the crystalline phase of the PAN nanofibers. The lithium ion and C=O groups of carbonate solvents then interacted with the C≡N groups of PAN. The XRD patterns of the PAN-based gel polymer electrolytes using the lithium salt-based electrolyte showed a single broad peak at about 20°.[10] Therefore, the strong peak at 21° in the electrospun PAN-based fibrous polymer electrolyte should be assigned to the disordered structure due to the interaction between the PAN and electrolyte solutions. The sharp peak at 17° remained, however, because the crystal structure of the PAN was not seriously broken down by the swelling of the electrospun PAN-based fibrous membrane, although the peaks at 28 and 55° were no longer observed. This may indicate that the three-dimensional network structure and the mechanical strength of fibrous membranes are maintained after their impregnation with the electrolyte solution.

In the PAN-based gel electrolyte, the peaks were shifted up and became much broader due to the enhanced swelling of the crystal phase. After 150 cycles, the electrospun PAN-based fibrous polymer electrolyte also showed very broad peaks compared with the situation before the cycle test. This indicates the enhanced swelling of the electrospun PAN-based nanofiber due to the electrochemical reaction during the cycle test.

In the PAN-based polymer electrolyte with the lithium-salt-based electrolyte, the interaction between $Li^+$ and PAN was much weaker than that between $Li^+$ and the solvent molecules, such as EC, DMC, DEC, and EMC. As such, the associated $Li^+$-PAN peak was very weakly observed in the FT-Raman spectra.[16-19] Figure 3 shows the FT-Raman spectra of the stretching mode of the C≡N groups in the electrospun PAN-based fibrous membrane, their fibrous polymer electrolytes that were aged for 12 h at 50°C, and the PAN-based gel electrolyte with 1 M $LiPF_6$-EC/DMC (1/1). The associated $Li^+$-PAN peaks in the fibrous polymer electrolytes were very weakly observed, but the expended spectra of Fig. 3b obviously shows a new weak peak due to the interaction between the lithium ion and the -C≡N group of PAN, which weakly appeared at around 2265 $cm^{-1}$. The diameters of the swollen PAN nanofibers in the fibrous polymer electrolyte did not significantly increase even after a cyclic performance of about 100 cycles, as Fig. 1a-c shows. This indicates a low ratio of $Li^+$:-CN in the solid fibrous phase of the PAN-based fibrous polymer electrolyte membrane, unlike in the conventional gel electrolyte.

Figure 3 also shows the FT-Raman spectra of the electrospun PAN-based fibrous polymer electrolyte after about 150 cycles, and of the conventional PAN-based gel polymer electrolyte, for comparison. For the fibrous polymer electrolyte, after 150 cycles, a strong peak of the $Li^+$-PAN association was observed at around 2270 $cm^{-1}$. This peak was shown in the PAN-based gel electrolyte was much stronger than that of the electrospun PAN fibrous polymer electrolyte. As shown in Fig. 1d, the electrochemical reaction during the cyclic performance of about 150 cycles remarkably enhanced the swelling of the PAN nanofibers, after which the diameters of the swollen PAN significantly increased. From these results, it can be said that the peak of the $Li^+$-PAN association largely depends on the number of PAN chains associated with the lithium ion. A significant swelling of the PAN in the case of both the electrospun fibrous polymer electrolyte and the gel polymer electrolyte is thought to induce an increase in the associated $Li^+$-PAN. On the other hand, the enhanced swelling of the solid phase of the PAN in the polymer electrolyte may result in a rapid decrease in the free CN peak and an increase in the association between $Li^+$ and the -CN of PAN. Both the electrospun fibrous polymer electrolyte after 150 cycles and the gel polymer electrolyte showed an increase in their associated $Li^+$-PAN peaks, but their free CN peaks did not decrease. In the PAN-based solid electrolytes, the intensity and position of the associated $Li^+$-PAN peak and -CN free band have been known to be greatly affected by the $Li^+$:-CN mole ratio and the counter anion type of lithium salt.[20,21] The CN peaks at around 2244 $cm^{-1}$ in the pure polymer were shifted up to about 2275 $cm^{-1}$ due to the association with $Li^+$. The lithium-salt-poor solid electrolytes showed a weak intensity of their associated $Li^+$-CN peaks. The relative intensity of the associated $Li^+$-CN peak in the $LiCF_3SO_3$/PAN (N:Li = 1.2:1) electrolyte was more intense, however, than that of the free -CN band at around 2244 $cm^{-1}$, whereas for the $LiClO_4$/PAN (N:Li = 1.1:1) electrolyte, the free band was dominant. This means that the $LiCF_3SO_3$ salt is considerably more soluble in PAN compared with both $LiClO_4$ and $LiN(CF_3SO_2)_2$. For the PAN-based fibrous polymer electrolyte, organic solvents dissociated the lithium salts and swelled the solid polymer. They also competed with the -CN of the PAN in the formation of a complex with the lithium salts. Therefore, the vibration mode of the -CN moieties for the electrospun PAN-based fibrous polymer electrolyte may be less sensitive to interaction with the cation of lithium salts than that of the PAN-based solid electrolyte. Moreover, the content of lithium salt in the swollen fibrous polymer electrolytes may be very low. Therefore, the above FT-Raman behavior of free CN and the associated $Li^+$-PAN after the cycle test were further investigated.

Figure 4 shows the FT-Raman spectra of the electrospun PAN-based fibrous membranes impregnated with the EC/DMC (1/1) solvent and the 1 M $LiPF_6$-EC/DMC (1/1) electrolyte. In the EC/DMC (1/1) solvent, two bands appeared at 893 and 916 $cm^{-1}$, which were assigned to a symmetric ring breathing mode of free EC molecules, and to a $CH_3$-O stretching mode of DMC molecules, respectively.[22,23] When the electrospun PAN-based fibrous membrane was introduced into the EC/DMC (1/1) solvent, the intensity of the $CH_3$-O stretching mode of DMC molecules remarkably decreased, but its position hardly changed. There was a strong dipole-dipole interaction between the C≡N groups of the PAN chains and the C=O groups of the EC and DMC molecules. The cyclic ring strain of the EC molecule is thought to resist the dipole-dipole interaction with PAN, however, although the DMC with a linear molecular chain interacted with PAN.

In the case of the 1 M $LiPF_6$-EC/DMC (1/1) electrolyte, new peaks were observed at around 905 and 931 $cm^{-1}$, corresponding to the $Li^+$-O = C interactions of EC and DMC, respectively. The EC molecule more easily solvated the lithium ion than did DMC because the dielectric constant of EC at 25°C is much higher than that of DMC, as listed in Table I.[24,25] As such, the band for the $Li^+$-EC interaction is larger than that for the $Li^+$-DMC.

The vibrational modes of the electrospun PAN-based fibrous polymer electrolyte with 1 M $LiPF_6$-EC/DMC (1/1) look like different bands from those of the above mentioned other samples. It still, however, reflects a very low affinity of PAN towards $Li^+$- that is, that EC molecules solvate lithium ion and DMC molecules interact with PAN. This also supports the Raman behavior of free CN and the associated $Li^+$-PAN peaks of the fibrous polymer electrolyte after 150 cycles, as shown in Fig. 3. From these results, it can be said that DMC molecules mainly penetrate into the PAN nanofiber, and that swollen PAN nanofibers do not contribute significantly to lithium ion transport. On the other hand, EC molecules interact with both lithium ions and PAN, and may thus have significantly influenced the ionic conductivity of the electrospun PAN-based fibrous polymer electrolytes.

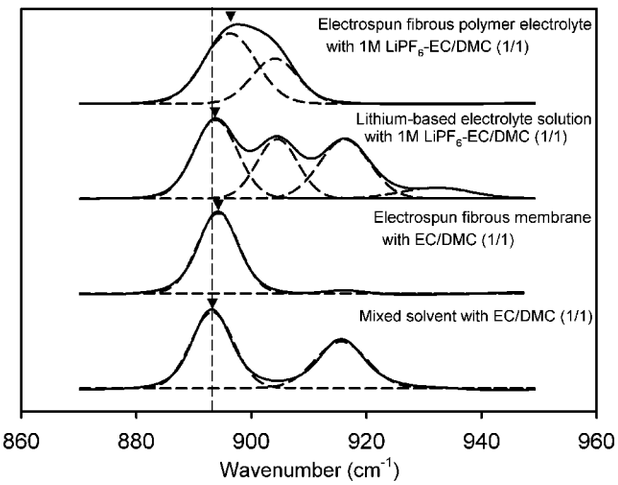


**Figure 4.** The normalized FT-Raman spectra of the EC symmetric ring breathing mode and the $CH_3$-O stretching mode of 1 M $LiPF_6$-EC/DMC (1/1) and EC/DMC (1/1) in the presence of an electrospun PAN fibrous membrane.

Figure 5 shows the ring bending mode of the C=O groups in the EC molecules in the 1 M $LiPF_6$-EC/DMC (1/1) solution and its fibrous polymer electrolyte. The ring bending mode of free EC, its associated $Li^+$-EC, and the free $PF_6^-$ counteranion in the fibrous electrolyte were observed at about 717-718, 724-726, and 742 $cm^{-1}$, respectively, whereas it generally appeared at 715 $cm^{-1}$ in the pure EC solvent.[26] Table II shows the relative area ratios of the ring bending modes of the associated $Li^+$-EC to the free EC in various electrolyte solutions and electrospun PAN-based fibrous polymer electrolytes. In the case of both electrolyte solutions and their fibrous polymer electrolytes, the relative area ratio of the associated $Li^+$-EC molecules to the free EC molecules decreased in the order of 1 M $LiPF_6$-EC/DMC/DEC (1/1/1) > 1 M $LiPF_6$-EC/DMC (1/1) > 1 M $LiPF_6$-EC/EMC (1/1) > 1 M $LiPF_6$-EC/DEC (1/1) > 1 M $LiPF_6$-EC/DMC (2/1). The relative area of the associated $Li^+$-EC was highest in the 1 M $LiPF_6$-EC/DMC/DEC (1/1/1) solution and lowest in the 1 M $LiPF_6$-EC/DMC (2/1) solution, because the 1 M $LiPF_6$ in these electrolyte solutions was almost completely dissociated. The 1 M $LiPF_6$-

**Table I. Physical properties of several carbonate solvents in lithium salt-based electrolyte solutions.**

| Carbonate solvent | EC | DMC | EMC | DEC |
|---|---|---|---|---|
| Structure | Cyclic | Linear | Linear | Linear |
| Melting point (°C) | 36.4 | 4.6 | −53 | −74.3 |
| Viscosity (cP at 25°C) | 1.93 | 0.589 | 0.648 | 0.753 |
| Dielectric constant at 25°C | 89.8 | 3.11 | 2.96 | 2.81 |

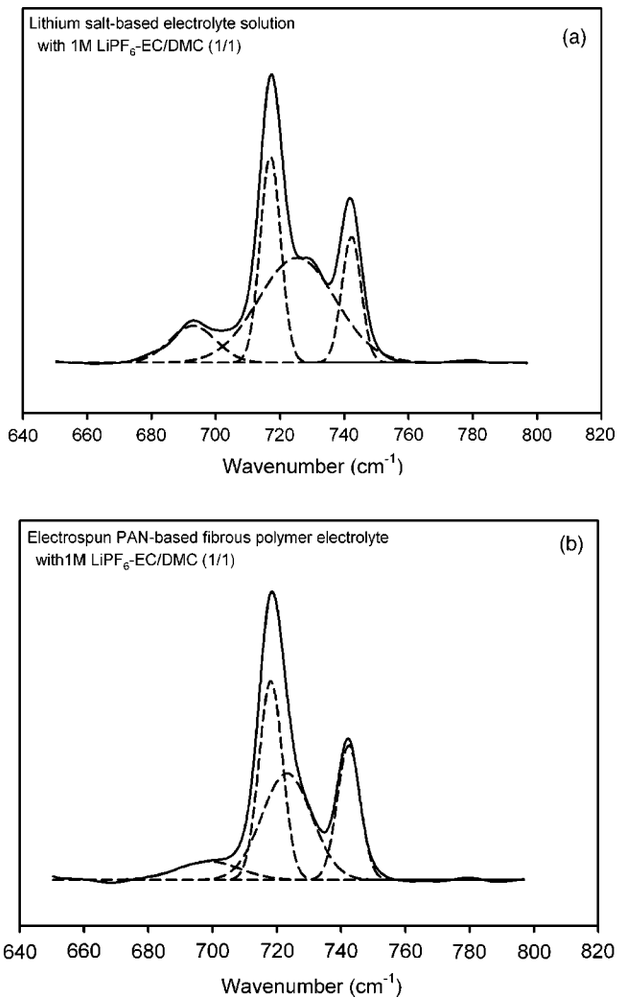


**Figure 5.** The FT-Raman spectra of the C=O bending mode in the electrolyte solution and the electrospun PAN-based fibrous polymer electrolyte with 1 M $LiPF_6$-EC/DMC (1/1).

EC/DMC (1/1) solution had the highest relative area of the associated $Li^+$-EC among the same weight fraction of alkyl carbonate due to its highest dielectric constant. The -CN group of PAN also showed a weak interaction with the $Li^+$ ion and the EC, so that the relative area ratios of the associated $Li^+$-EC molecules in the electrospun PAN-based fibrous polymer were smaller than those in the electrolyte solutions themselves. The increase in the EC content in the electrolyte solutions resulted in an increase in the free EC molecules and in a complex number of EC molecules to $Li^+$, indicating a decrease in the mobility of the associated $Li^+$-EC molecules, or an increase in electrolyte viscosity.

**Table II. Relative area ratios of the ring bending mode of EC in electrolyte solutions and electrospun PAN-based fibrous polymer electrolytes.**

| | Relative area ratio ($A_{Li^+\text{-EC}}/A_{\text{free EC}}$) | |
|---|---|---|
| 1 M $LiPF_6$ electrolyte solutions | Electrolyte solutions | Fibrous polymer electrolytes |
| EC/DMC (2/1) | 1.48 | 0.75 |
| EC/DMC (1/1) | 2.05 | 1.13 |
| EC/EMC (1/1) | 2.01 | 1.06 |
| EC/DEC (1/1) | 1.85 | 0.99 |
| EC/DMC/DEC (1/1/1) | 2.38 | 1.35 |

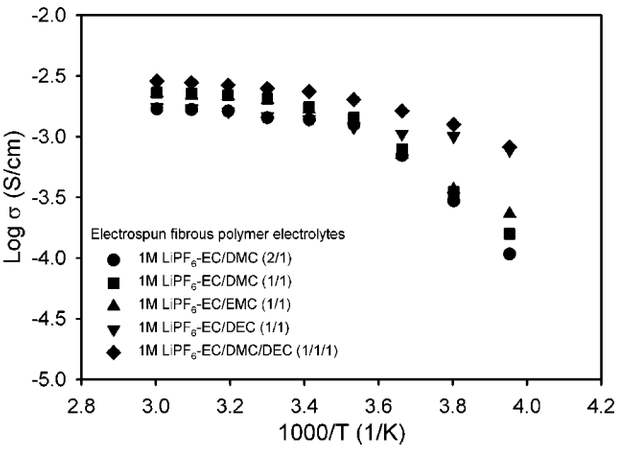


**Figure 6.** Ionic conductivities of electrospun PAN-based fibrous polymer electrolytes.

The associated $Li^+$-EC molecules are thought to have directly affected the ionic conductivity of the electrolyte solution because these complexes moved through the interconnected pores of the fibrous electrolyte membrane. It is supposed that the ionic conductivity increased with the increase in the molecules' mobility.

The ionic conductivities of electrospun PAN-based fibrous polymer electrolytes are shown in Fig. 6. In addition to a slow ion conduction path in the swollen PAN nanofiber phase, the solvated lithium ions moved through interconnected pores of the electrospun PAN fibrous membrane. The size and tortuosity of the pores in the polymer electrolyte can be very important factors in determining the effectiveness of ion conduction. Therefore, the ionic conductivities of the electrospun PAN fibrous polymer electrolytes were lower than those of the electrolyte solvents themselves because of their slow conduction path in the swollen fiber phase and the tortuosity of the pore structure of the PAN fibrous polymer electrolytes. The ionic conductivities of the electrospun PAN-based polymer electrolytes increased with temperature and was above $1.0 \times 10^{-3}$ S/cm at room temperature. Their behavior in the low-temperature region of −20 to 10°C depended, however, on the freezing property of carbonate solvents in the electrolyte solution, and decreased with the increase in the EC content in the electrolyte solution, because the crystalline part of EC hinders lithium ion transport. The fibrous polymer electrolyte with 1 M $LiPF_6$-EC/DMC/DEC (1/1/1) showed the highest ionic conductivity, whereas that with 1 M $LiPF_6$-EC/DMC (2/1) showed the lowest ionic conductivity. As shown in Table I, the solidification temperature of the solvent mixture was expected to decrease in the order of EC/DMC > EC/EMC > EC/DEC at the same weight fraction of EC, because the linear carbonate solvent suppressed the solidification of the EC. In the case of the electrospun PAN-based fibrous polymer electrolytes, therefore, which contained linear carbonate solvents of the same weight fraction, the ionic conductivities also decreased in the order of EC/DEC > EC/EMC > EC/DMC.

Electrolyte solutions in the high-temperature region (20-60°C) fully formed liquid phases. The ionic conductivities of the electrospun PAN-based fibrous polymer electrolytes showed high ionic conductivities of above $1.0 \times 10^{-3}$ S/cm above room temperature, and decreased in the order of 1 M $LiPF_6$-EC/DMC/DEC (1/1/1) > 1 M $LiPF_6$-EC/DMC (1/1) > 1 M $LiPF_6$-EC/EMC (1/1) > 1 M $LiPF_6$-EC/DEC (1/1) > 1 M $LiPF_6$-EC/DMC (2/1). The ionic conductivity depended on the mobility and the number of associated $Li^+$-EC molecules. The electrolyte solutions with a higher EC con-

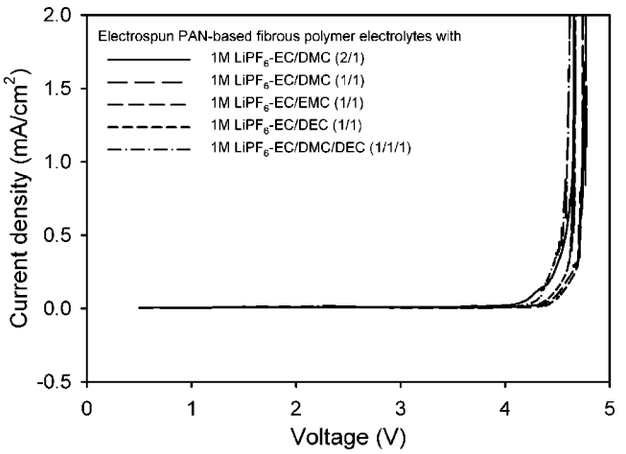


**Figure 7.** Electrochemical stability windows of electrospun PAN-based fibrous polymer electrolytes.

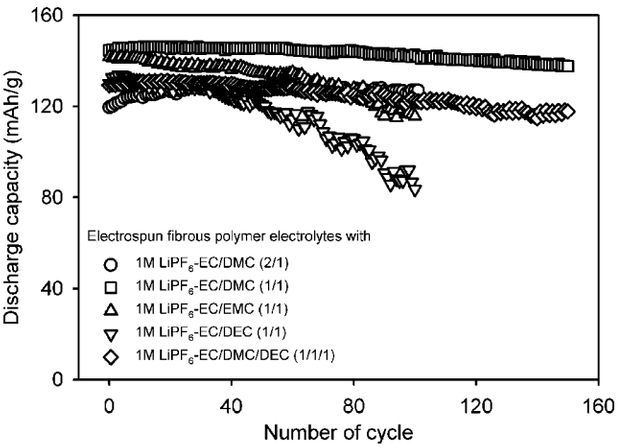


**Figure 8.** Cycle performances of graphite/electrospun PAN-based fibrous polymer electrolytes and $LiCoO_2$ cells at 0.5C/0.5C rate of charge/discharge condition.

tent had a lower ionic conductivity due to their higher viscosity. In the fibrous polymer electrolytes, the lithium ion was mainly solvated by the EC solvent, whereas the linear carbonate solvent swelled the PAN polymer, as shown in Fig. 4. Thus, the mobility of the associated $Li^+$-EC in the fibrous polymer electrolytes was depressed more significantly than that of the electrolyte solution itself. The fibrous polymer electrolyte with a higher EC content showed a lower ionic conductivity because the mobility of the lithium ion was depressed due to the high viscosity of EC. From these results, it can be said that the ionic conductivities of the electrospun PAN-based fibrous polymer electrolytes depended mainly on the physicochemical properties of the electrolyte solution filled with pores.

Figure 7 shows the electrochemical stability of the electrospun PAN-based fibrous polymer electrolytes. Although the electrospun PAN fibrous membrane has large pores and high porosity, the fibrous polymer electrolytes showed a high electrochemical stability of up to 4.5 V. The gel phase of the polymer electrolyte generally allowed an increase of the anodic limit voltage to up to 0.6 V compared with that of the electrolyte itself.[27] In the case of the electrospun PAN fibrous membranes, they showed a high affinity with and a good swelling ability for the electrolyte solution. The swollen phase of the electrospun PAN-based fibrous polymer electrolyte included complex components, such as the associated $Li^+$-N≡C- group, the associated $Li^+$-O=C group, and the associated C≡N-$Li^+$-O=C group. The electrochemical stability of the resulting fibrous polymer electrolyte is thought to have been greatly enhanced by its complex formation with the lithium ion and the dipole-dipole interaction between the C≡N groups of PAN and the C=O groups of the carbonate molecules. Therefore, electrospun PAN-based fibrous polymer electrolytes are expected to be stable within the operating voltage of a lithium polymer battery.

The discharge capacities of graphite/electrospun PAN-based fibrous polymer electrolytes/$LiCoO_2$ cells are shown in Fig. 8. The cells were cycled between 4.20 and 2.75 V at a constant current (1.7 mA/cm$^2$ at the 0.5C rate). The prototype cells were subjected to preconditioning with a cutoff voltage of 4.20-2.75 V at 0.67 mA/cm$^2$ (at the 0.2C rate) for the initial five cycles before the cycling test. In this experiment, it is estimated that the theoretical capacity of the $LiCoO_2$ electrode is 145 mAh/g. Solvent molecules have been known to cointercalate as the associated form of $Li^+$ into graphite layers during charging.[28,29] Such solvent cointercalation took place more extensively in the EC/DEC system than in the EC/DMC system because the DEC molecules enhanced the cointercalation of the solvent. The cointercalated solvent molecules were not easily released from the graphite electrode, and were transformed into inactive materials that formed a passivation layer during their charge/discharge performances. Irreversible capacities of the EC/DEC system in the first and second cycles were thus larger than those of the other system because the EC/DEC system showed a more inhomogeneous passivation layer than did the EC/DMC system. In the case of the EC/DMC electrolyte system, the prototype cell is expected to show a cycle performance superior to that of the EC/DEC system.

In an experiment conducted in relation to this paper, the prototype cell with 1 M $LiPF_6$-EC/DMC (1/1) showed the highest discharge capacity and the most stable cyclic performance among all the electrolyte solvents. It showed an initial discharge capacity of 145 mAh/g and 94.1% of the initial discharge capacity after 150 cycles at the charge/discharge rate of 0.5C/0.5C. The prototype cell with polymer electrolyte containing 1 M $LiPF_6$-EC/DMC (2/1) showed a very good cyclic performance and retained 98.5% of its maximum discharge capacity after 100 cycles. It was, however, a lower discharge capacity of 129 mAh/g compared to that with 1 M LiPF6-EC/DMC (1/1). This might have been due to the lower mobility of the lithium ion compared to that of the polymer electrolyte with 1 M $LiPF_6$-EC/DMC (1/1), indicating a low ionic conductivity. On the other hand, the prototype cells with other electrolyte solvents showed a low discharge capacity and an unstable cyclic performance because the DEC readily cointercalated into the graphite negative electrode. The prototype cell with 1 M $LiPF_6$-EC/DEC (1/1) showed the worst cyclic performance, and 62.5% of the initial discharge capacity after 100 cycles. In the case of the prototype cell with 1 M $LiPF_6$-EC/EMC (1/1), its discharge capacity was similar to that with 1 M $LiPF_6$-EC/DMC (1/1) in the first few cycles, but decreased during the cycle test, like that with 1 M $LiPF_6$-EC/DEC (1/1). It has thus been confirmed that EMC is less cointercalated than DEC. As such, the prototype cell with 1 M $LiPF_6$-EC/EMC (1/1) shows slower capacity fading than that with 1 M $LiPF_6$-EC/DEC (1/1) and 81.7% of the initial discharge capacity after 100 cycles. The prototype cell with 1 M $LiPF_6$-EC/DMC/DEC (1/1/1) showed a lower discharge capacity than that with 1 M $LiPF_6$-EC/DMC (1/1) but a cycle performance similar to that with 1 M $LiPF_6$-EC/DMC (2/1). Although its discharge capacity very slowly decreased during the cycling test because the amount of its DEC was relatively low, its discharge capacity slowly faded and showed 89.2% of its initial discharge capacity after 150 cycles. From these results, it is thought that the cycle performance of prototype cells with electrospun PAN fibrous polymer electrolytes is also influenced by the properties of electrolyte solutions. The electrospun PAN fibrous polymer electrolyte

with 1 M $LiPF_6$-EC/DMC (1/1) after 150 cycles showed the most probable cycle property for lithium polymer batteries.

## Conclusion

An electrospun PAN fibrous membrane is an attractive porous polymer matrix that has three-dimensional network structures with micropores and large porosity. The average fiber diameter of the electrospun PAN-based fibrous polymer electrolyte in the prototype cell after 150 cycles remarkably increased by about three times compared with before the cycling test. The swelling behavior of the electrospun PAN-based fibrous polymer electrolytes had some effects on the electrochemical properties and the cycling performance of the prototype cell with the electrospun PAN-based fibrous polymer electrolyte. In the vibrational spectra, the PAN interacted mainly with the linear alkyl carbonate molecules, and then formed a gel phase that enhanced the electrochemical properties of fibrous polymer electrolyte. On the other hand, the lithium ions predominantly associated with the ethylene carbonate molecules, after which the $Li^+$-solvated EC became a major path of lithium ion transport.

The ionic conductivities of the electrospun PAN-based fibrous polymer electrolytes were above $1.0 \times 10^{-3}$ S/cm at room temperature. The ionic conductivity depended on the interaction of $Li^+$ and the C=O group of EC molecules and their mobility in the liquid phase. It was also partially enhanced by the interaction between $Li^+$ and the C≡N group of PAN.

The interaction of $Li^+$ and the C=O group of carbonate molecules and that between $Li^+$ and the C≡N group affected the other electrochemical properties of fibrous polymer electrolytes. The electrochemical stability was also enhanced by the swelling of the electrolyte solution due to the dipole-dipole interaction between the C≡N groups of PAN and the C=O groups of the carbonate molecules. Therefore, electrochemical stability windows are stable up to 4.5 V and are suitable for applications of lithium-ion polymer batteries.

In the lithium salt-based electrolyte solution, solvent molecules have been known to cointercalate as the associated form of $Li^+$ into graphite, and to form a passivation layer during their charge/discharge performances. The prototype cells based on the electrospun PAN fibrous polymer electrolyte with 1 M $LiPF_6$-EC/DMC (1/1) showed the most stable cycling performance after 150 cycles because their DMC molecules might have been less cointercalated into the graphite anode during the charging step than were the EMC or DEC molecules. The prototype cells showed an initial discharge capacity of 145 mAh/g and 94.1% of the initial discharge capacity after 150 cycles at a charge/discharge rate of 0.5C/0.5C.

## Acknowledgments

This work was financially supported by the Ministry of Commerce, Industry, and Energy of Korea and the Nanofiber R&D Center of Samshin Creation Co. in Korea.

*Korea Institute of Science and Technology assisted in meeting the publication costs of this article.*

## References

1. J. Y. Song, C. L. Cheng, Y. Y. Wang, and C. C. Wan, *J. Electrochem. Soc.*, **149**, A1230 (2002).
2. Y. Saito, H. Kataoka, and A. M. Stephan, *Macromolecules*, **34**, 6955 (2001).
3. W. Xu, K. S. Siow, Z. Gao, and S. Y. Lee, *J. Electrochem. Soc.*, **146**, 4410 (1999).
4. H.-S. Min, J.-M. Ko, and D.-W. Kim, *J. Power Sources*, **119-121**, 469 (2003).
5. Z. Wang, B. Huang, H. Huang, L. Chen, R. Xue, and F. Wang, *Solid State Ionics*, **85**, 143 (1996).
6. I. Nicotera, C. Oliviero, G. Ranieri, A. Spadafora, M. Castriota, and E. Cazzanelli, *J. Chem. Phys.*, **117**, 7373 (2002).
7. T.-C. Wen, H.-H. Kuo, and A. Gopalan, *Macromolecules*, **34**, 2958 (2001).
8. D. Ostrovskii, A. Brodin, L. M. Torell, G. B. Appetecchi, and B. Scosati, *J. Chem. Phys.*, **109**, 7618 (1998).
9. D.-W. Kim, Y.-R. Kim, J.-K. Park, and S.-I. Moon, *Solid State Ionics*, **106**, 329 (1998).
10. B. Hunag, Z. Wang, L. Chen, R. Xue, and F. Wang, *Solid State Ionics*, **91**, 279 (1996).
11. A. Magistris, P. Mustarelli, F. Parazzoli, E. Quartarone, P. Piaggio, and A. Bottino, *J. Power Sources*, **97-98**, 657 (2001).
12. T. Michot, A. Nishimoto, and M. Watanabe, *Electrochim. Acta*, **45**, 1347 (2000).
13. S. W. Choi, S. M. Jo, W. S. Lee, and Y.-R. Kim, *Adv. Mater. (Weinheim, Ger.)*, **15**, 2027 (2003).
14. J. Li, X. Huang, and L. Chen, *J. Electrochem. Soc.*, **147**, 2653 (2000).
15. M. Sokól and E. Turska, *Acta Polym.*, **35**, 135 (1984).
16. Z. Wang, B. Huang, R. Xue, X. Huang, and L. Chen, *Solid State Ionics*, **121**, 141 (1999).
17. Z. Wang, W. Gao, L. Chen, Y. Mo, and X. Huang, *J. Electrochem. Soc.*, **149**, E148 (2002).
18. Z. Wang, W. Gao, X. Huang, Y. Mo, and L. Chen, *Electrochem. Solid-State Lett.*, **4**, A148 (2001).
19. H. Akashi, K.-I. Tanaka, and K. Sekai, *J. Electrochem. Soc.*, **145**, 881 (1998).
20. A. Ferry, L. Edman, M. Forsyth, D-R. MacFarlane, and J. Sun, *Electrochim. Acta*, **45**, 1237 (2000).
21. A. Wang, B. Huang. S. Wang, R. Xue, X. Huang, and L. Chen, *J. Electrochem. Soc.*, **144**, 778 (1997).
22. R. Aroca, M. Nazri, G. A. Nazri, A. J. Camargo, and M. Trsic, *J. Solution Chem.*, **29**, 1047 (2000).
23. B. Klassen, R. Aroca, M. Nazri, and G. A. Nazri, *J. Phys. Chem. B*, **102**, 4795 (1998).
24. M. S. Ding, K. Xu, and T. R. Jow, *J. Electrochem. Soc.*, **147**, 1688 (2000).
25. M. S. Ding, K. Xu, and T. R. Jow, *J. Electrochem. Soc.*, **148**, A299 (2001).
26. M. Morita, Y. Asai, N. Yoshimoto, and M. Ishikawa, *J. Chem. Soc., Faraday Trans.*, **94**, 3451 (1998).
27. M. Moshkovich, M. Cojocaru, H. E. Gottlieb, and D. Aurbach, *J. Electroanal. Chem.*, **497**, 84 (2001).
28. S.-K. Jeong, M. Inaba, Y. Iriyama, T. Abe, and Z. Ogumi, *Electrochim. Acta*, **47**, 1975 (2002).
29. C. R. Yang, J. Y. Song, Y. Y. Wang, and C. C. Wan, *J. Appl. Electrochem.*, **30**, 29 (2000).